ADVANCES IN ATMOSPHERIC SCIENCES, VOL. 31, JULY 2014, 765–778

Regional-scale Surface Air Temperature and East Asian Summer Monsoon Changes during the Last Millennium Simulated by the FGOALS-gl Climate System Model

MAN Wenmin[1,2] and ZHOU Tianjun*[1,3]

[1]*State Key Laboratory of Numerical Modeling for Atmospheric Sciences and Geophysical Fluid Dynamics, Institute of Atmospheric Physics, Chinese Academy of Sciences, Beijing* 100029

[2]*Key Laboratory of Meteorological Disaster of Ministry of Education, Nanjing University of Information Science and Technology, Nanjing* 210044

[3]*Climate Change Research Center, Chinese Academy of Sciences, Beijing* 100029

(Received 18 June 2013; revised 27 November 2013; accepted 6 December 2013)

ABSTRACT

The spatial patterns and regional-scale surface air temperature (SAT) changes during the last millennium, as well as the variability of the East Asian summer monsoon (EASM) were simulated with a low-resolution version of Flexible Global Ocean–Atmosphere–Land–Sea-ice (FGOALS-gl) model. The model was driven by both natural and anthropogenic forcing agents. Major features of the simulated past millennial Northern Hemisphere (NH) mean SAT variations, including the Medieval Climate Anomaly (MCA), the Little Ice Age (LIA) and the 20th Century Warming (20CW), were generally consistent with the reconstructions. The simulated MCA showed a global cooling pattern with reference to the 1961–90 mean conditions, indicating the 20CW to be unprecedented over the last millennium in the simulation. The LIA was characterized by pronounced coldness over the continental extratropical NH in both the reconstruction and the simulation. The simulated global mean SAT difference between the MCA and LIA was 0.14°C, with enhanced warming over high-latitude NH continental regions. Consistencies between the simulation and the reconstruction on regional scales were lower than those on hemispheric scales. The major features agreed well between the simulated and reconstructed SAT variations over the Chinese domain, despite some inconsistency in details among different reconstructions. The EASM circulation during the MCA was stronger than that during the LIA The corresponding rainfall anomalies exhibited excessive rainfall in the north but deficient rainfall in the south. Both the zonal and meridional thermal contrast were enhanced during the MCA. This temperature anomaly pattern favored a stronger monsoon circulation.

Key words: last millennium, surface air temperature, spatial patterns, regional-scale variation, East Asian summer monsoon

Citation: Man, W. M., and T. J. Zhou, 2014: Regional-scale surface air temperature and East Asian summer monsoon changes during the last millennium simulated by the FGOALS-gl climate system model. *Adv. Atmos. Sci.*, **31**(4), 765–778, doi: 10.1007/s00376-013-3123-y.

1. Introduction

The recently observed episode of global warming has promoted studies of climate evolution over the last millennium. In addition to the warming due to increased concentrations of greenhouse gases during the past century, previous studies indicate that both solar irradiance and volcanic eruptions have contributed to climate variations over the last millennium (Lean et al., 1995; Overpeck et al., 1997; Crowley, 2000). To understand the behavior of recent temperature change and its mechanisms, parallel efforts should be devoted to assessing the climate of earlier times and factors that might influence the past climate.

Due to insufficient instrumental measurements over pre-industrial times, considerable progress has been made by using climate "proxy" data to reconstruct climate variations in past centuries. A number of annually-resolved reconstructions representing Northern Hemisphere (NH) mean temperature changes over the last millennium have been published in recent years (Mann et al., 1999; Esper et al., 2002; Cook et al., 2004; Moberg et al., 2005; Rutherford et al., 2005; D'Arrigo et al., 2006; Hegerl et al., 2007; Kaufman et al., 2009; Ljungqvist, 2010). These records are not entirely independent reconstructions but in general they span two climatologically interesting periods during pre-industrial times, the so-called "Medieval Climate Anomaly" (MCA) (or "Medieval Warm Period"; MWP) and "Little Ice Age" (LIA),

* Corresponding author: ZHOU Tianjun
Email: zhoutj@lasg.iap.ac.cn

which correspond to relatively warm and cold conditions, respectively.

In addition to the temporal evolution of temperature change over the last millennium, a better understanding of the spatial patterns of temperature change could be even more important to see variations on regional scales (Mann et al., 2009). However, less progress has been made in identifying the spatial patterns of those changes due to the sparseness of the available proxy data. Owing to the inherent uncertainties of the proxy data and the specific statistical methods used for scaling them to represent past temperatures, debate exists regarding the robustness and quality of temperature reconstructions over the last millennium (Christiansen et al., 2009; Smerdon et al., 2010).

Climate models are useful tools for understanding climate changes. Comparisons of model simulations with proxy reconstructions have the potential to enrich our knowledge of millennialscale climate change. Many climate models with different levels of complexity are able to reproduce the evolution of global and hemispheric mean surface air temperature (SAT) changes during the last millennium when driven by historical radiative forcings (Crowley, 2000; Bertrand et al., 2002; Bauer et al., 2003; Gerber et al., 2003; González-Rouco et al., 2003; Goosse et al., 2005; Zorita et al., 2005; Osborn et al., 2006; Ammann et al., 2007; Liu et al., 2009; Peng et al., 2009; Jungclaus et al., 2010; Servonnat et al., 2010). Roles of solar irradiance and the radiative effects from volcanic eruptions have also been investigated based on model results. However, in comparison with the abundant simulations of the 20th century climate (Zhou and Yu, 2006; Zhou et al., 2013), the number of millennial-scale climate simulations is quite limited. More importantly, due to either model or forcing data uncertainty, the existing simulations show large differences among models (Fernandez-Donado et al., 2013).

A 1000-yr transient simulation was recently conducted with the coupled climate system model developed by the State Key Laboratory of Numerical Modeling for Atmospheric Sciences and Geophysical Fluid Dynamics/Institute of Atmospheric Physics (LASG/IAP), Chinese Academy of Sciences (Man and Zhou, 2011). Based on this transient simulation, Zhang et al. (2013) examined the global/hemispheric mean surface air temperature responses and indicated that total external forcing can explain about half of the climate variance during the whole millennium period. To understand the strengths and limitations of this millennial-scale simulation, the energy balance, climate sensitivity and absorption feedback of the model were also analyzed (Guo and Zhou, 2013). However, the spatial patterns and regional-scale temperature changes during the last millennium as well as the variability of the East Asian summer monsoon (EASM) were not examined. Thus the main motivation of the present study was to address the following questions: (1) What are the spatial patterns and regional-scale SAT changes during the MCA and LIA? (2) What is the level of consistency between the simulated SAT changes over the Chinese domain and various reconstructions? (3) What are the differences in the EASM variations between the MCA and LIA? (4) What are the dominant reasons for the centennial EASM variations?

The remainder of the paper is organized as follows. Descriptions of the model and the experimental design, as well as details of the forcing agents used in the simulation are described in section 2. The spatial patterns of SAT changes and the EASM variations during the last millennium are assessed in section 3. And finally, section 4 provides a summary and a discussion of the key findings.

2. Model and data

2.1. *Model*

The coupled model used in this study was the fast version of the LASG/IAP Flexible Global Ocean–Atmosphere–Land–Sea ice (FGOALS) model FGOALS is a fully-coupled model that has four individual components, including atmospheric, oceanic, land and sea ice models, coupled together by the National Center for Atmospheric Research Community Climate System Model (NCAR CCSM2) coupler (Zhou et al., 2008). The atmospheric component of FGOALS employs a lowresolution version of the Grid Atmospheric Model of IAP/LASG (GAMIL) and is thus referred to as FGOALSgl. The low-resolution version of GAMIL has a 72×40 weighted equal-area mesh, which corresponds approximately to a 5° (lon) $\times 4.5^\circ$ (lat) grid, with 26 vertical levels in a sigma coordinate. In GAMIL, the physical parameterizations are taken from the NCAR Community Atmosphere Model (CAM2) (Wen et al., 2007). The LASG/IAP Climate Ocean Model (LICOM), which has a horizontal resolution of $1^\circ \times 1^\circ$, with 30 levels in the vertical direction, is employed as an oceanic component in the coupled model (Liu et al., 2004). The other two components of FGOALS-gl, including the sea ice model and the land model, are taken from NCAR CCSM2 (Bonan et al., 2002; Briegleb et al., 2004). In FGOALS-gl, during the coupled integration, the correction of freshwater fluxes and heat exchanged at the interfaces among the aforementioned four coupled components are not considered. For more details of FGOALS-gl, readers are referred to Zhou et al. (2008).

2.2. *Experimental design and forcing data*

A 100-yr control run was firstly performed under AD 1000 external forcing conditions. Starting from the oceanic initial conditions derived from a 500-yr spin-up integration for present-day conditions (Liu et al., 2004) a simulation spanning the time AD 1000 to 1999 was conducted using FGOALS-gl (Zhang et al., 2013). The model was driven by both natural (solar irradiance and volcanic eruptions) and anthropogenic (greenhouse gases and sulfate aerosols) forcing agents. The simulation did not include anthropogenic land-use changes or orbital variations

The individual forcing factors used in driving the model were the same as in Peng et al. (2009). Both the solar irradiance and volcanic forcing data were from Crowley et al. (2003). The long-term variations of this relatively "old" ver-

sion of solar irradiance are larger than the recent "state of the art" estimates for solar variability (Schmidt et al., 2011). The increase from the Maunder Minimum to present was about 0.18% in this study, while the recent PMIP3 (phase three of the Paleoclimate Modelling Intercomparison Project) simulations used increases $\leqslant$0.10 %. The effect of volcanic eruptions was applied as a negative deviation from the solar radiation. The latitudinal dependence of volcanic aerosol was not taken into account in this study, although more recent simulations have incorporated the effects of volcanic eruptions in a more sophisticated manner. The greenhouse gas concentrations (CO_2, CH_4 and N_2O) were from Ammann et al. (2007). The influence of tropospheric sulfate aerosols was taken into account from AD 1850 and the aerosol data were from CMIP3 (phase three of the Coupled Model Intercomparison Project) (Zhou and Yu, 2006).

2.3. *Data for model comparisons*

The reconstruction data of Mann et al. (2009), based on a multi-proxy network for the last 1500 years, were used in the model comparisons. The proxy dataset was calibrated using the $5.0^\circ \times 5.0^\circ$ temperature gridded dataset of the Climate Research Unit (CRU) of the University of East Anglia, and thus the methodology resulted in reconstructed gridded temperature fields. Records of NH mean temperature variations with yearly resolution during the last millennium from IPCC AR4 (fourth Assessment Report of the Intergovernmental Panel on Climate Change) (Jansen et al., 2007) were used to benchmark the simulation at hemispheric scales. As the reconstruction data from Mann et al. (2009) and Jansen et al. (2007) are anomalies relative to the climate mean of the 1961–90 reference period, in the present study the anomalies in the simulation were calculated with respect to the 1961–90 mean at hemispheric scales as well as in the spatial patterns for the model-reconstruction comparisons.

In addition to global and hemispheric reconstructions, the following reconstruction data for China were also used:

(1) Annual mean SAT data for the last millennium from Wang et al. (2007) (hereafter referred to as "Wang-data"), which were established by merging proxy records of several subregions by a specific area weight. This dataset has a comprehensive spatial coverage compared with other reconstructions in China.

(2) Annual mean SAT data covering the last 2000 years from Yang et al. (2002) (hereafter referred to as "Yang-data"), which were constructed by combining China-wide multiple paleoclimate proxy records.

(3) The 10–30-yr resolution, winter half-year (October-April) temperatures for the past 2000 years from Ge et al. (2003) (hereafter referred to as "Ge-data"), which were reconstructed by using Chinese historical documents in the central region of eastern China.

(4) A 2650-yr (BC 665–AD 1985) warm season (May–August) temperature reconstruction from Tan et al. (2003) (hereafter referred to as "Tan-data"), which was derived from annual layers of a stalagmite from Shihua Cave, Beijing, China.

3. Results

3.1. *NH mean SAT changes*

The simulated NH mean SAT changes during the last millennium are firstly presented to evaluate the model performances (Fig. 1). The reconstructed NH mean temperature variations using multiple climate proxy records are presented as in Fig. 6.10 of Jansen et al. (2007) for model comparisons. The anomalies were calculated relative to the climate mean of the 1961–90 reference period. According to the reconstructions, the 20th century was the warmest century of the

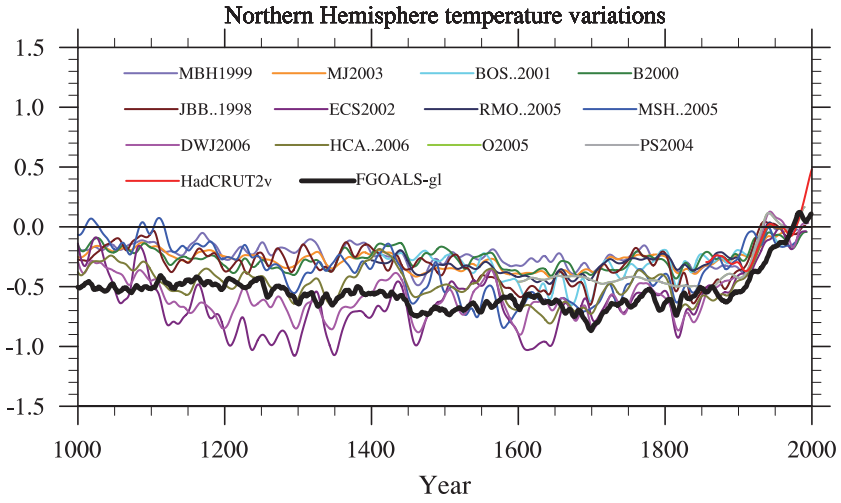

Fig. 1. Low-pass filtered NH mean SAT changes (°C) during the last millennium. Reconstructed NH mean temperature variations from IPCC AR4 are presented as in Fig. 6.10(b) of Jansen et al. (2007). The simulated time series is shown by the black line. The anomalies have been calculated with respect to the climate mean of the 1961–90 reference period.

last millennium. Based on the mean of the reconstructions, temperature during the MCA was about 0.2°C lower than the reference climate, while the LIA was about 0.4°C colder relative to the recent climatology. Good agreements were seen between the simulated NH mean SAT time series and the reconstructions. Warm anomalies in the first centuries as well as cool anomalies in intermediate time periods were evident in the simulation. The warm conditions at the end of the 20th century were unprecedented in the context of the last millennium. The simulated SAT anomalies fell well within the uncertainty range of the reconstructions during the MCA, although there were relatively large uncertainties at the beginning of the millennium, which could be attributed to the weak model sensitivity to natural forcing in FGOALS-gl (Guo and Zhou, 2013).

3.2. *Spatial patterns of SAT*

In this study, we defined the MCA and LIA as AD 1000 to 1300 and AD 1400 to 1700, respectively. The spatial patterns of SAT for the MCA and LIA are compared in Fig. 2. The reconstructed MCA pattern (Fig. 2a) was characterized by warm conditions (∼ 0.05°C–0.3°C, with the highest value up to 1°C) over a large part of the North Atlantic, the Eurasian Arctic, the North Pacific, and parts of North America, exceeding that of the warming in recent decades. The warming in the North Pacific during the MCA was consistent with a La Niñalike pattern in the tropical Pacific, which shows a strong cooling in the eastern tropical Pacific and a warming in the western tropical Pacific. The rest of the world exhibited cooling anomalies relative to recent conditions The LIA pattern (Fig. 2c) featured a pronounced cooling over NH continents, with a central value of about −0.5°C; but in some regions such as parts of the central North Atlantic, Africa, parts of North America tropical Eurasia, and the extratropical Pacific Ocean, warm anomalies comparable to those of the present day were evident.

The simulation showed a broad-scale cooling pattern over much of the globe during the MCA relative to the climate mean of the 1961–90 reference period (Fig. 2b). The warm conditions over certain regions in the reconstruction were not evident in the simulation. Part of the North Pacific was dominated by a warming signal as in the reconstruction. The simulated global mean SAT during the MCA was −0.26°C with respect to the 1961–90 mean. The model response was stronger than the reconstruction (−0.26°C versus −0.16°C, respectively). The simulated LIA exhibited a uniform cooling pattern with an enhanced cooling over NH continental regions (Fig. 2d). The global mean SAT anomaly during the LIA was −0.40°C relative to the 1961–90 mean condition. This was close to the anomaly derived from the reconstruction, which was −0.38°C.

A useful metric for evaluating the results of the last millennial climate simulation is the difference in SAT between the MCA and the LIA. As shown in Fig. 3a, the reconstruction exhibited a La Niñalike pattern in the tropical Pacific for the MCA-LIA differences (Cobb et al., 2003; Mann et al., 2005; Graham et al., 2007). Another prominent feature was the enhanced warm conditions over interior North America and the Eurasian Arctic, with amplitudes ranging from 0.6°C to 0.9°C, and coldness with amplitude of −0.15°C over central Eurasia. The SAT pattern indicated a positive phase of the North Atlantic Oscillation (NAO), which was consistent with the high-index state of NAO during the MCA and the low-index state during the LIA in the simulation

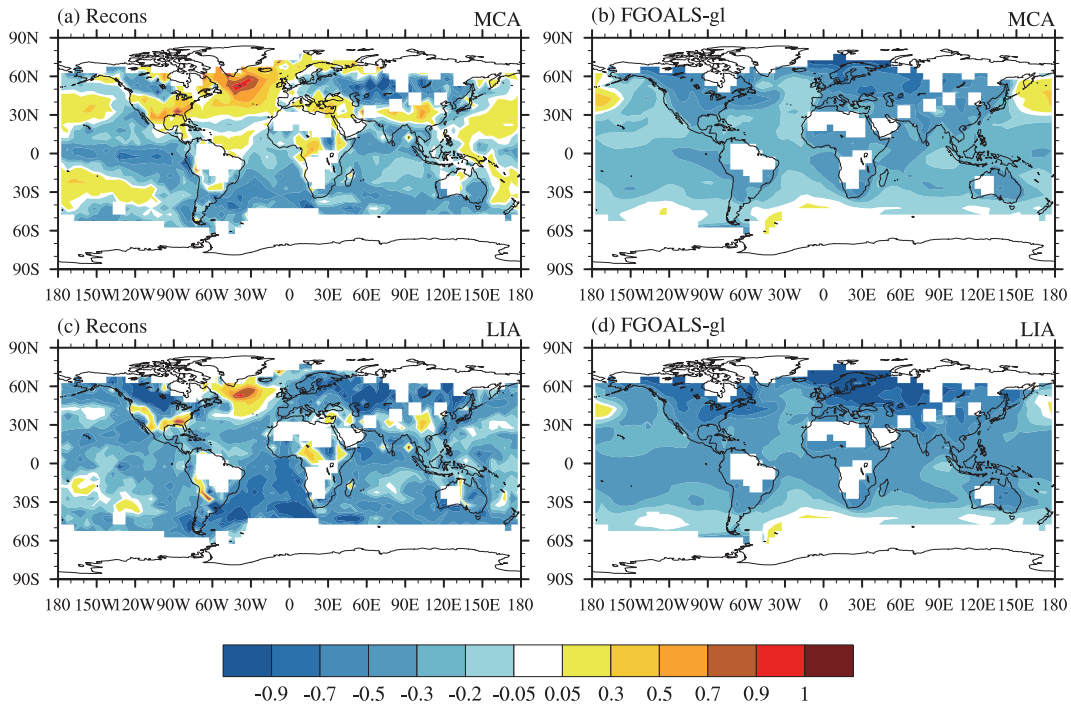

Fig. 2. Reconstructed and simulated SAT patterns (°C) for (a, b) MCA (AD 1000–1300) and (c, d) LIA (AD 1400–1700). Anomalies have been defined relative to the 1961–90 reference period mean.

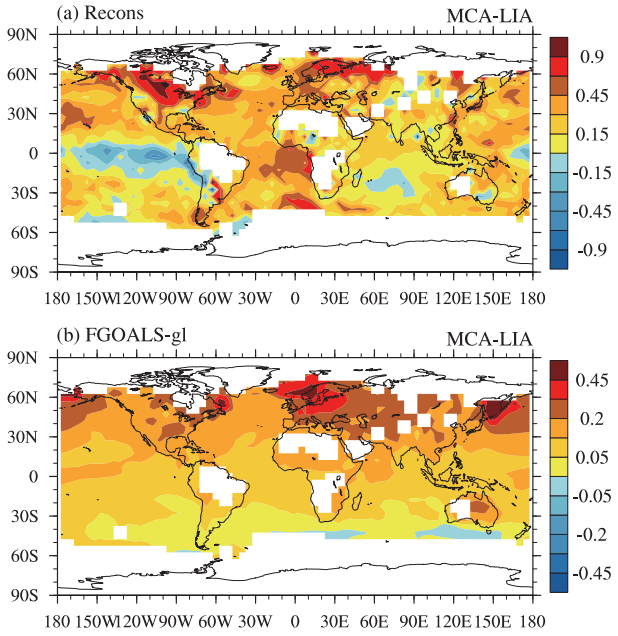

Fig. 3. Spatial patterns of the MCA–LIA SAT difference (°C) for (a) the reconstruction and (b) model simulation (using the same MCA and LIA time intervals as defined above). The reconstructed mask has been applied to the model patterns for ease of comparison.

(Man and Zhou, 2011), and such a pattern has been found in paleoclimate reconstructions of the last millennium (Jones and Mann, 2004; Trouet et al., 2009).

In the simulation (Fig. 3b), the global mean SAT difference between the MCA and LIA was 0.14°C, which was comparable to or slightly weaker than the reconstruction value of 0.22°C. The La Niña-like conditions were not evident in the simulation Such a pattern has been reproduced in simulations (Mann et al., 2005) employing the simplified Zebiak-Cane model of the tropical Pacific coupled ocean-atmosphere system (Zebiak and Cane, 1987), which exhibits a stronger dynamical feedback than most global models. The FGOALS-gl model roughly reproduced the reconstructed pattern of enhanced warming over North America and Arctic Eurasia, but the intensity was weaker than the reconstruction.

3.3. *Regional-scale SAT changes*

Previous paleoclimatic reconstructions on regional scales have suggested that the timing and intensity of the climate epochs of the MCA and LIA differed geographically (Jones and Bradley, 1992; Hughes and Diaz, 1994). Since the proxy records are mainly located over land (Mann et al., 2009), to reveal regionalscale features of SAT changes, the global land area was divided into 21 regions The definitions of these regions over land in terms of latitude and longitude followed those of Giorgi and Francisco (2000).

Various regional-scale temperature changes during the last millennium are shown in Fig. 4. Each of the time series was the moving average by a 31-yr sliding window and screened with the reconstructed data coverage for the region. In the tropics, all simulated curves showed reasonable agreement with the reconstructions, including eastern and western Africa, the Sahel, southern Asia, Southeast Asia and Central America, with correlation coefficients all exceeding 0.5 (statistically significant at the 5% level). Over the Sahara and Central America, the simulation was generally colder than the reconstruction prior to the 20th century.

At higher latitudes of the NH, especially from 30°N to 85°N, the reconstructed series exhibited evident multidecadal and centennial fluctuations with warming conditions during the early centuries and a cooling trend over the LIA as well as an abrupt strong warming during the 20th century. The model generally showed good agreement with the reconstructed series in Alaska, western North America and Asian regions (northern, central, and eastern Asia). However, the simulation exhibited a smaller range of variability on centennial time scales prior to the 20th century. The simulation was generally colder than the reconstruction in central North America, eastern North America, Greenland, northern Europe and the Mediterranean. The cold bias suggested that although the coupled model is able to reproduce the hemispheric-scale SAT variations, it is still a challenge to accurately reproduce regional-scale SAT variations. The deficiency of the global model in reproducing regional-scale SAT change during the last millennium is consistent with most CMIP3 models in simulating the 20th century SAT changes (Zhou and Yu, 2006).

In the Southern Hemisphere (SH), the models showed reasonable performances in the regions of the Amazon, western and eastern Africa, and Australia. In some other regions, such as the southern part of South America and South Africa, the simulated centennial variation was not so robust and the simulation was generally warmer than the reconstruction.

The above comparison indicates that the level of consistency between simulations by FGOALS-gl and reconstructed data on regional scales is generally lower than that on hemispheric scales. This may be due to the increasing internal variability at local scales (Yoshimori et al., 2005) Ensemble experiments are needed in future work to show the signal-to-noise ratio and reveal the robustness of the model response to external forcings.

We further focus on the regional SAT changes during the MCA and LIA periods. As shown in Fig. 5a, among the 21 regions, only four regions including central North America, eastern North America, Greenland and the Mediterranean exhibited warming anomalies over the MCA relative to recent conditions in the reconstruction. In the simulation, however, all 21 regions were dominated by cooling anomalies, indicating the natural MCA warming to still be colder than the anthropogenic 20th century warming. During the LIA, in both the reconstruction and the simulation, all regions saw colder anomalies except for region 9 (Greenland) in the reconstruction (Fig. 5b). The model bias in Greenland is partly due to the higher model sensitivity of FGOALS-gl in the industrial era than that of the pre-industrial period (Guo and Zhou, 2013) as well as the strong sea-ice feedback in the model (Man et al., 2011). The comparison indicates that the model-

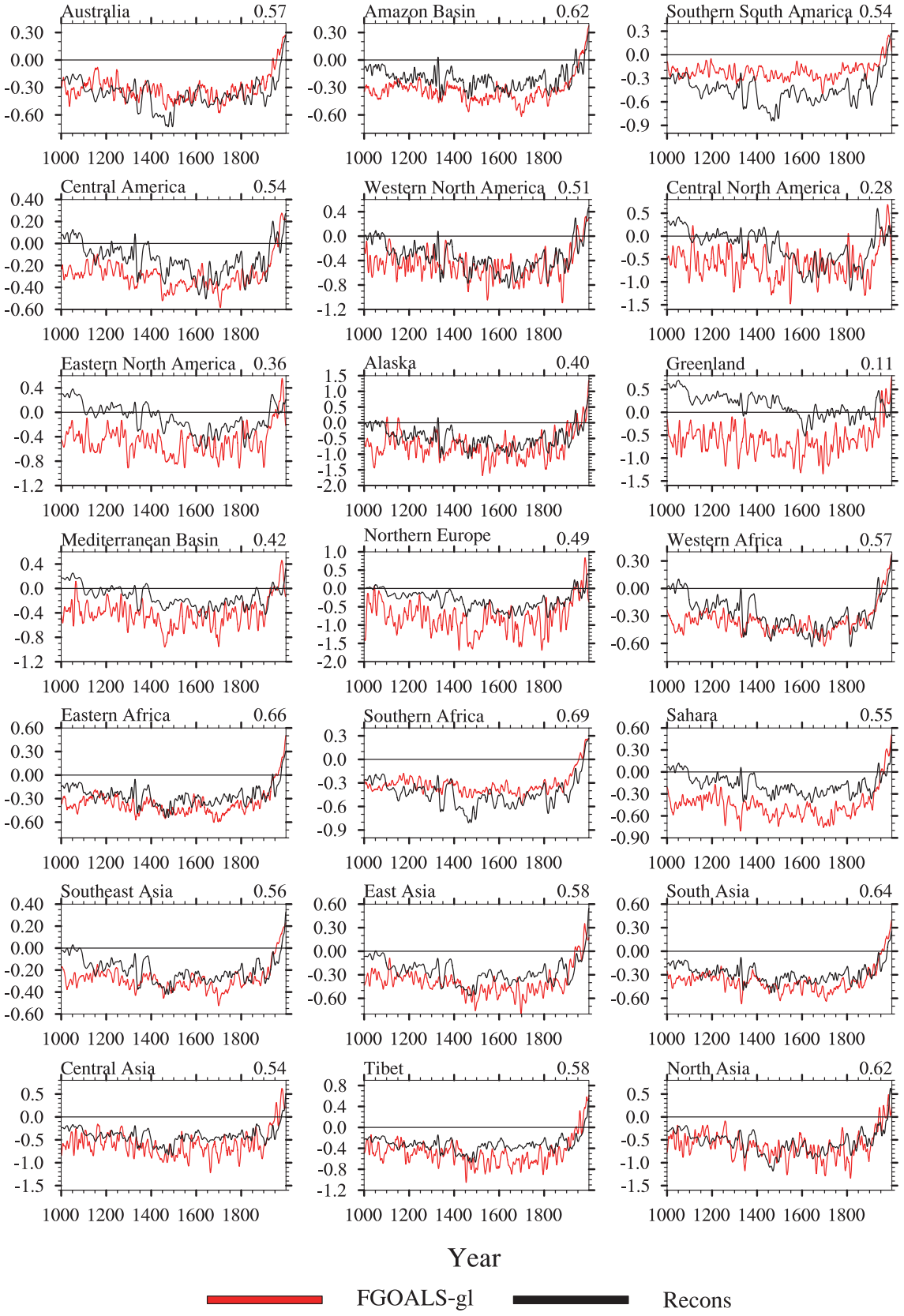

Fig. 4. Time series of annual mean SAT changes (°C) for the 21 regions over global land area. Each of the time series has been screened with a 31-yr low-pass filter and calculated relative to the climate mean of the 1961–90 period Black and red curves denote the reconstruction and the simulation, respectively. The value is the correlation coefficients between the simulated and reconstructed SAT series for the 21 regions.

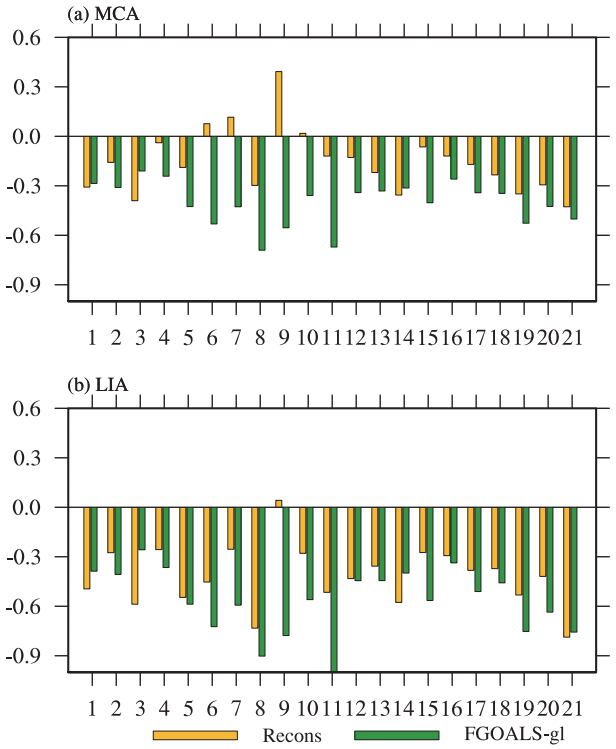

Fig. 5. Comparisons of mean (a) MCA and (b) LIA SAT anomalies (°C) of the 21 sub-regions between the reconstructions (yellow bars) and the simulations (green bars).

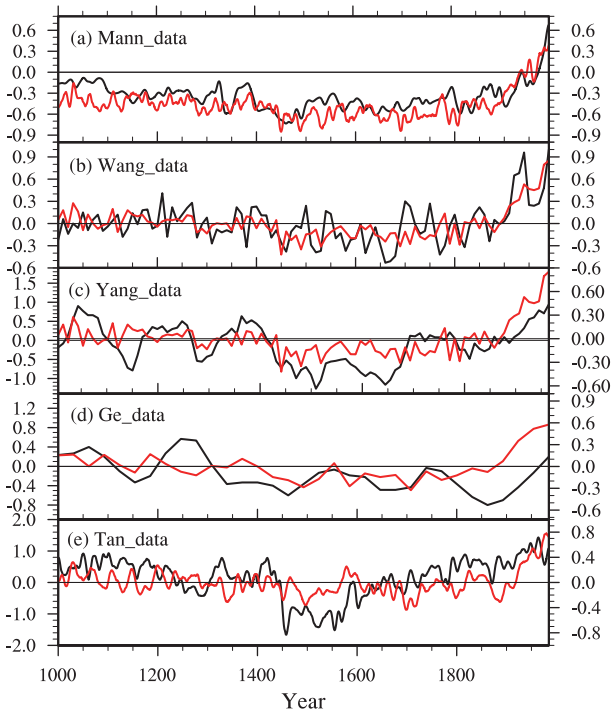

Fig. 6. Comparisons of the simulated (red line) and the reconstructed (black line) SAT series (°C) over the Chinese domain: (a) Mann-data; (b) Wang-data; (c) Yang-data; (d) Ge-data; (e) Tan-data. The simulated SAT anomalies have been rescaled to the timescales of each corresponding reconstruction: the anomalies for Mann-data and Tan-data are annual mean values and smoothed with a 31-yr low-pass filter, while the anomalies have been processed to 10-yr intervals for the Wang-data and Yang-data and 30-yr intervals for the Ge-data. The value in the left column indicates the reconstructed SAT anomalies, while that in the right column indicates the simulated SAT anomalies.

reconstruction consistency for the LIA is better than that for the MCA. This was further evidenced by the same-sign ratios between the simulation and the reconstruction in the 21 regions, which was 81% for the MCA and 95% for the LIA.

3.4. *SAT changes over China*

Several sets of millennial SAT reconstruction data for the Chinese domain have been provided in recent years (Yang et al., 2002; Ge et al., 2003; Tan et al., 2003; Wang et al., 2007). It is desirable to carry out model-proxy data comparisons over the region. Note that both Wang-data and Yang-data are in 10-yr intervals, while Ge-data is in 30-yr intervals The simulations were rescaled to the timescales of each corresponding reconstruction before we performed the simulation-reconstruction comparisons. The simulated time series were for the same seasons as the reconstructions The simulated SAT anomalies were also calculated relative to the base period of each reconstruction. Among the reconstructions, both the timing and magnitude of major warm/cool periods showed differences (Fig. 6) Both the Mann-data and Wang-data exhibited warm conditions over AD 1000–1300 and cold conditions over AD 1400–1850. The Yang-data and Ge-data exhibited a cold spell over AD 1100–1200. A notable warming period between AD 1300 and 1400 was found in the Yang-data and Tan-data, followed by a short cooling period prior to AD 1600 in the Tan-data, but prior to AD 1700 in the Yang-data. The Yang-data and Tan-data exhibited larger amplitudes of variability than the other records, with standard deviations of 0.52 and 0.63, respectively. The corresponding standard deviations of Mann-data, Wang-data, and Ge-data were 0.19, 0.27 and 0.36 (units: °C), respectively.

Despite the inconsistency between the reconstructions, agreement was found regarding the major features over China: a warm stage during AD 1000–110 and AD 1200-1300; the cold LIA period during AD 1400–170; and the present warming stage over the 20th century. The simulated SAT series showed general agreement with the reconstructions for the last millennium, which displayed obvious warming during most of AD 1000–1300, with lower temperatures being sustained during AD 1450–1800, and the subsequent warming to unprecedented levels at the end of the 20th century. As shown in Table 1 the correlation coefficients (statistically significant at the 5% level) between the simulated and the reconstructed series all exceeded 0.5 for the last millennium. It should be noted that the original samples were hereafter adjusted to the effective sample size according to Dawdy and Matalas (1964) when performing the statistical test. The coincidence between the simulation and the reconstructions suggested that external forcing may play an important role in SAT variations over China.

The correlation coefficients over the three typical time periods of the last millennium [the MCA, LIA and the 20th

Table 1. Correlation coefficients between the simulated and reconstructed SAT series over China. Bold numbers are statistically significant at the 5% level. The reconstruction from Ge et al. (2003) was not included because of the low sampling resolution.

	Mann et al. (2009)	Wang et al. (2007)	Yang et al. (2002)	Tan et al. (2003)
AD 1000–2000	**0.70**	**0.61**	**0.55**	**0.54**
MCA	0.03	0.05	0.08	0.11
LIA	**0.17**	**0.21**	**0.41**	**0.42**
20CW	**0.92**	**0.58**	**0.85**	**0.55**

Century Warming (20CW)] were further examined (Table 1). The lowest correlation coefficients (statistically insignificant at the 5% level) were over the MCA and this may be partly due to large uncertainties in the proxy-based temperature reconstructions for the period prior to the 16th century (Ge et al., 2010). The consistency for LIA was better than that for the MCA. The highest correlation coefficients were over the 20th century, reaching 0.92 in the Mann-data. The low correlation coefficients during the MCA period may have arisen from the biases of both the simulation and the reconstruction.

The spectral peaks in reconstructions are shown in Figs 7a–e. A dominant spectral peak of 160 yr was evident in the

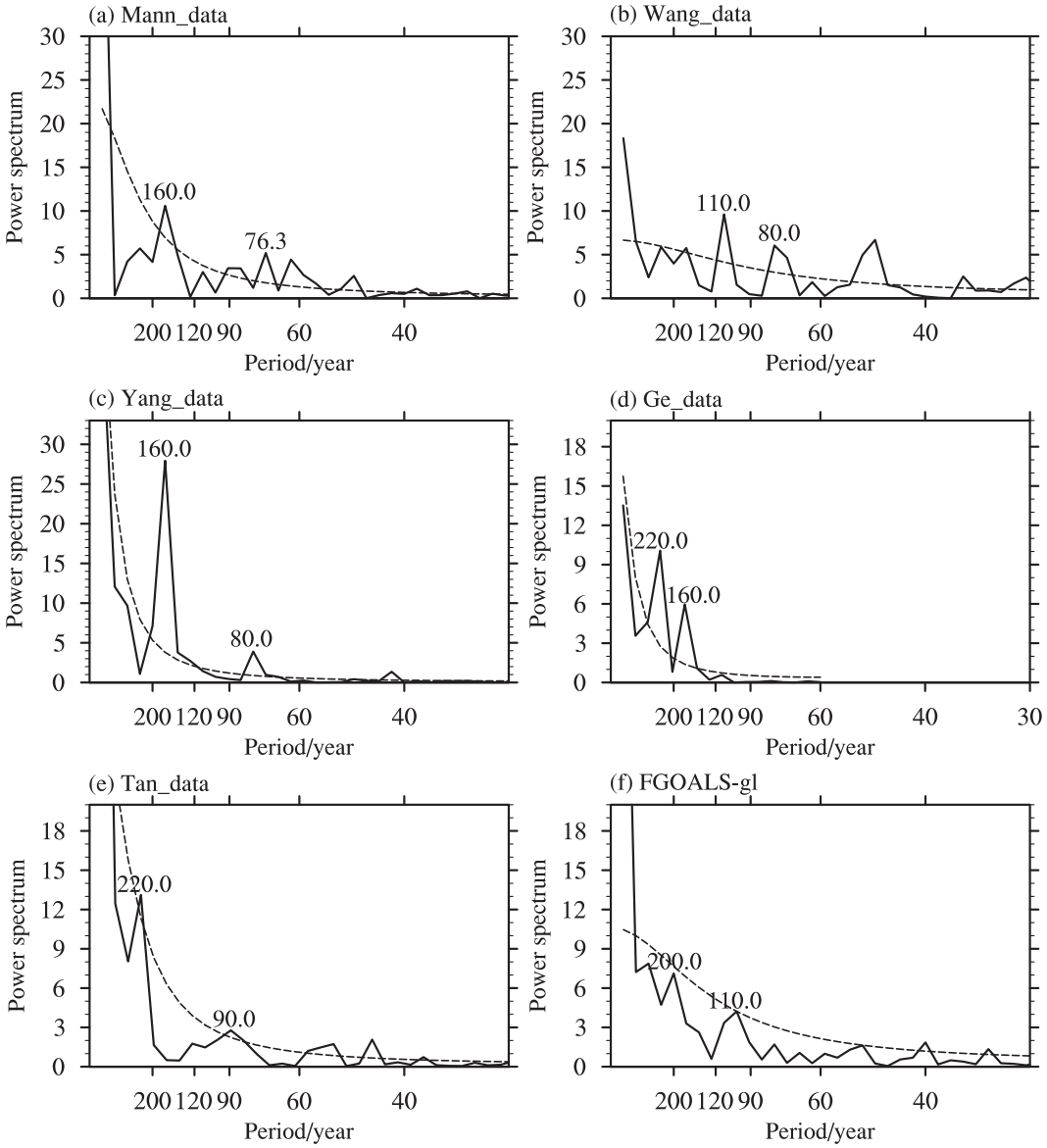

Fig. 7. Power spectra for the reconstructed and the simulated SAT series over the Chinese domain: (a) Mann-data; (b) Wang-data; (c) Yang-data; (d) Ge-data; (e) Tan-data; (f) model simulation. The time series were normalized prior to the spectrum analyses. Solid lines denote the spectrum; dashed lines denote the least-squares best fit of a theoretical red noise spectrum (Markov "Red Noise" spectrum).

Mann-, Yang-, and Ge-data, but was missing in the Wang- and Tan-data. The leading spectral peak was 220 yr in the Tan- and Ge-data. The Wang-data was dominated mainly by a major 110 yr peak. At sub-centennial time scales, a peak around 80 yr was evident in the Mann-, Wang-, and Yang-data. The corresponding spectral peak in the Tan-data was 90 yr. While nearly all the reconstructions exhibited a coherent peak around 80–90 yrs, the diversity of the reconstructions in revealing the spectral peaks longer than 100 yr indicated that it is beyond our ability to accurately measure the time scales of SAT variability over the Chinese domain based on current reconstructions, and thus more effort should be devoted to reconstructions in the near future. The major and secondary peaks in the simulation were 200 yr and 110 yr, respectively (Fig. 7f). This generally corresponded to the spectral peaks of specified effective solar radiation forgings.

3.5. *EASM variations during different climate epochs*

The performance of the model in monsoon simulation was evaluated in Zhou et al. (2011), and the results showed that the model can reasonably simulate the mean state of summer rainfall as well as the seasonal march of the monsoon rain belt. The centennialscale EASM variations were examined in the present study by evaluating the June–July–August (JJA) mean 850 hPa winds and precipitation difference between the MCA and LIA epochs (Fig. 8a). The East Asian continent was controlled by southerly wind anomalies, indicating a generally stronger EASM circulation during the MCA than that during the LIA. This result was consistent with the reconstruction from the stalagmite records (Zhang et al., 2008) and model results from the ECHO-G model (Liu et al., 2011) and the MPI Earth system model (Man et al., 2012). Previous analysis of the Asian-Pacific Oscillation also indicated a stronger EASM during the MCA and a weaker EASM during the LIA (Man and Zhou, 2011). The corresponding rainfall anomalies exhibited an out-of-phase change over East China, with more precipitation over North China but less precipitation over South China.

The monsoon circulation was mainly driven by land-sea thermal contrast. The spatial pattern of MCA-LIA SAT difference revealed a coherent warming over the East Asian continent (Fig. 8b). Due to different land-sea heat capacity, the warming over the land was stronger than that over the ocean. The temperature response suggested an enhanced land-sea thermal contrast, which would lead to southerly wind anomalies.

The corresponding structures through vertical cross sections are further shown in Fig. 9 to depict both the zonal and meridional land-sea thermal contrast. The zonal land–sea thermal contrast (Fig. 9a) exhibited "warmer-land" for the MCA-LIA temperature difference, with warmer anomalies of 0.2°C over the Eurasian continent extending from 60° to 120°E. The temperature over the ocean area was also warmer, but the magnitude was weaker than that over the land, and thus the land-sea thermal contrast was still enhanced. The meridional land-sea thermal contrast also exhibited a "warmer-land" structure for the MCA-LIA temperature

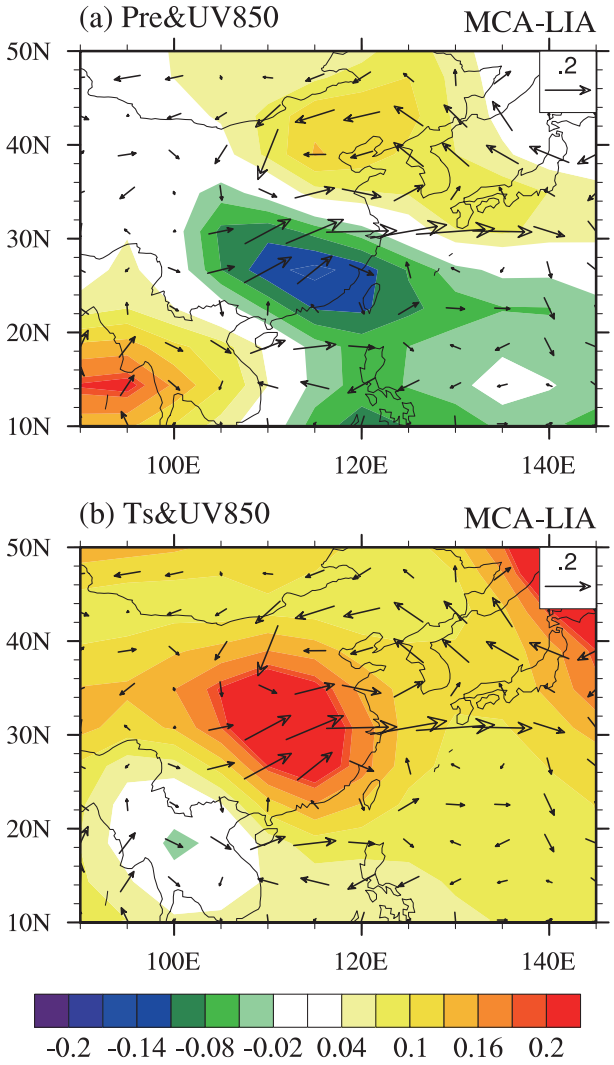

Fig. 8. The differences between MCA and LIA (MCA minus LIA) for (a) JJA mean precipitation (colored; units: mm d^{-1}) and 850 hPa winds (vectors; units: m s^{-1}), and (b) JJA mean surface air temperature (colored; units: °C) and 850 hPa winds (vectors; units: m s^{-1}).

difference (Fig. 9b). The "warmer land" structure was evident with its maximum warming of 0.3°C around 300–500 hPa extending from 30° to 45°N. There was coherent warming over the ocean, but the magnitude was much weaker than that over the land. The above results showed that both the zonal and the meridional thermal contrast were enhanced during the MCA, as compared to during the LIA. This temperature anomaly pattern would have favored a stronger monsoon circulation (Fig. 8).

In order to reveal the leading interannual variability mode of the EASM during different climate epochs, a combined Empirical Orthogonal Function (EOF) analysis was performed on the summer (May–September) mean precipitation and 850 hPa winds over East Asia. As shown in Fig. 10 (top panel), the 850 hPa wind anomalies featured an anticyclone over the East Asian monsoon area, and the corresponding

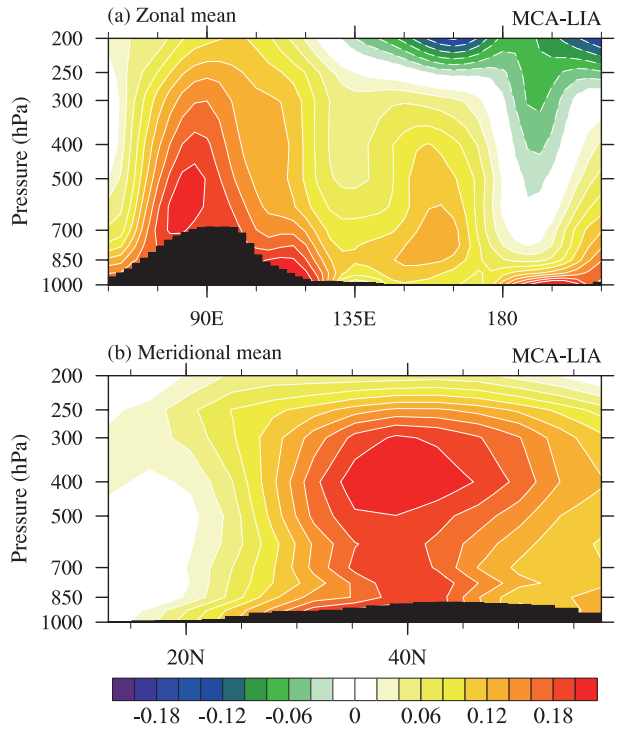

Fig. 9. (a) Longitude–height cross section of JJA temperature averaged over 30°–45°N and (b) latitude–height cross section of JJA temperature averaged over 105°–122°E (units: °C) for the difference between MCA and LIA (MCA minus LIA).

precipitation anomaly featured an out-of-phase change between North China and along the Yangtze River valley. The leading interannual modes of all the three typical climate epochs of the MCA, LIA, and 20CW showed similar characteristics. Since the mean climates of the MCA, LIA and 20CW were different, the similarity of the leading interannual variability modes among different climate epochs indicated that the impact of mean climate on the interannual variability of monsoon was negligible. A previous study suggested a different structure exists in the extratropical regions for the interannual variability mode under different background climates (Liu et al., 2011). This phenomenon was not found in our study, indicating that the results of the previous study may have been model-dependent.

Although the changes in the spatial anomaly pattern were similar in the MCA, LIA, and 20CW, differences were seen in the periodicity of the temporal variation of the leading EOF. As shown in Fig. 10 (bottom panel), the spectrum exhibited two peaks in the warm period, i.e., the 5-yr and 3.5-yr peaks in the MCA, and the 4-yr and 2.5-yr peaks in the 20CW. During the cold period of the LIA, there was only one peak at around 4 yr, while the biannual oscillation was not significant. These features were identical to those of MCA, LIA, and 20CW time-slice simulations (Zhou et al., 2011). It seems that the biannual oscillation of the EASM tends to be more prevalent in a warmer climate (Shen and Lau, 1995; Chang et al., 2000).

4. Summary and discussion

4.1. *Summary*

Spatial patterns and regional-scale SAT changes and the variability of the EASM during the past millennium were simulated with a climate system model (FGOALS-gl). The strengths and weaknesses of the simulation in comparison with reconstructed data as well as the implications of the results in terms of the underlying mechanisms of the EASM were discussed. The key findings can be summarized as follows:

(1) The reconstructed MCA pattern displayed warm conditions exceeding those of past decades in some regions, but was still colder than the recent reference climate. The MCA was marked by La Niña-like conditions in the tropical Pacific in the reconstruction, but this feature was not evident in the simulation. The simulated MCA displayed a broad-scale cooling pattern over much of the globe with reference to the 1961-90 mean conditions The LIA featured pronounced cooling over the extratropical continental NH in both the reconstruction and the simulation. The simulated global mean SAT difference between the MCA and LIA was 0.14°C (0.22°C for the reconstruction), with enhanced warming over continental North America and Eurasia.

(2) The consistencies between the simulated and reconstructed SAT changes on regional scales were generally lower than those on hemispheric scales. Regional SAT changes during the MCA and LIA periods indicated that all 21 subregions were dominated by cooling anomalies with reference to past decades in the simulation, with the same-sign ratios between the simulation and reconstruction being 81% for the MCA and 95% for the LIA.

(3) The major features agreed well among the five reconstructed datasets over the Chinese domain: a warm stage during AD 1000–110 and AD 1200–1300; the cold LIA period during AD 1400–170; and the present warming stage over the 20th century. The simulated SAT series over China showed general agreement with the reconstructions, although some differences in the timing and amplitude of SAT changes were also evident This suggested that the SAT changes over China may have been driven by the effective radiative forcing during the past millennium.

(4) At the centennial time scale, the structure between the MCA and LIA epochs (MCA minus LIA) featured strengthened 850 hPa southerly wind anomalies. The corresponding rainfall anomalies exhibited excessive rainfall over North China but deficient rainfall over South China. The monsoon circulation was driven by land-sea thermal contrast. Both the zonal and the meridional thermal contrast were enhanced during the MCA as compared to during the LIA. This temperature anomaly pattern favored a stronger monsoon circulation.

(5) A comparison of the interannual variability mode of the EASM during the MCA, LIA and 20CW revealed a similar rainfall anomaly pattern. However, the power spectra of the leading interannual variability modes during the three typical periods were different, and the biannual oscillation was most evident during warm periods.

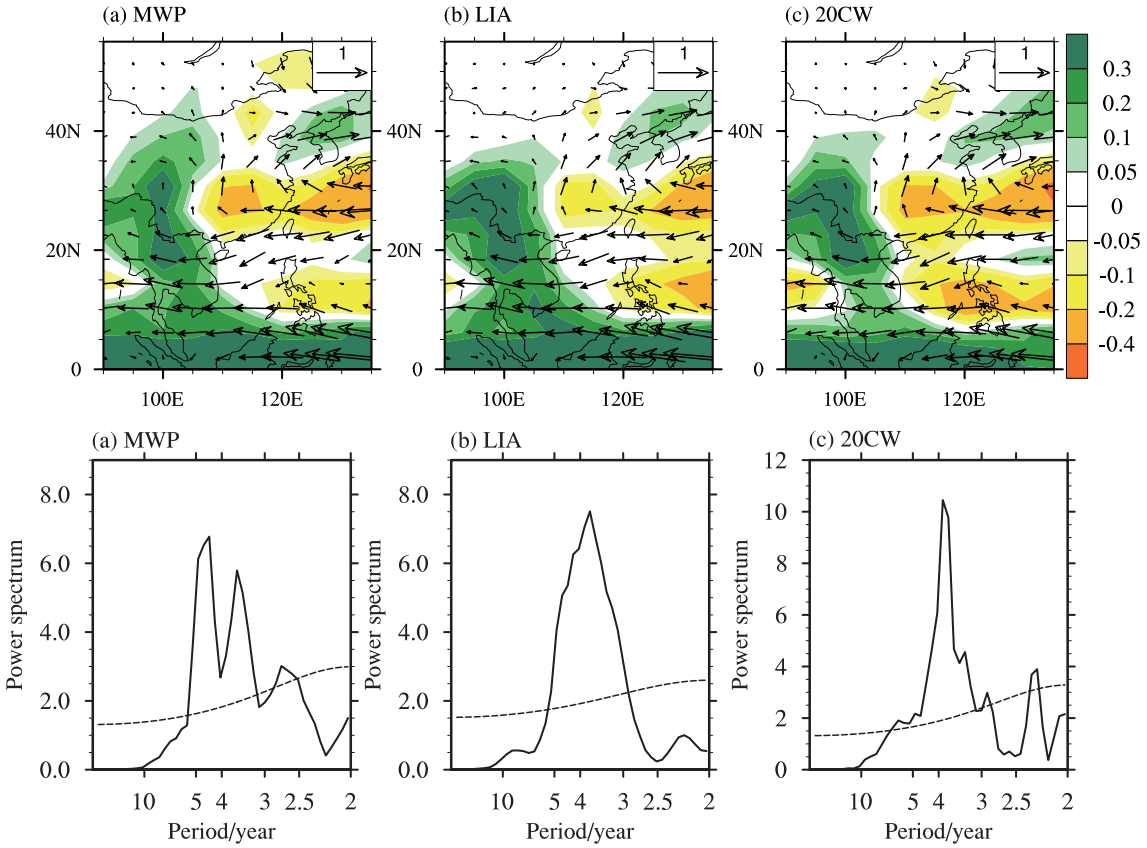

Fig. 10. The leading interannual variability mode of EASM [upper panel; shading is the precipitation anomaly (units: mm d^{-1})] and the vectors are wind anomalies at 850 hPa (units: m s^{-1})], and the spectra of the corresponding principal component time series [bottom panel (units of abscissa: yr); dashed line denotes the least-squares best fit of a theoretical red noise spectrum]: (a) MCA; (b) LIA; (c) 20CW.

4.2. *Discussion*

The present study revealed reasonable spatiotemporal patterns of temperature change during the last millennium; however, the simulation still showed some discrepancies relative to the reconstruction which were partly due to the coarse resolution of the model and also the uncertainties in estimates of past radiative forcings. The level of solar irradiance used to drive the model exhibits relatively larger change in comparison to that recently recommended by PMIP3 (http://pmip3.lsce.ipsl.fr/), and thus a smaller intensity of temperature variations is expected if the model is driven by solar irradiance with a smaller amplitude. We intend to rerun the simulation using the forcing data recommended by PMIP3 and the current results should serve as a useful reference for comparison.

It is difficult to interpret the simulated temperature in this study since it included both externally-forced and internal variability. Ensemble experiments are needed to show the model spread and enable us to see the robustness of the model responses. The coherence of spectral peaks between the global mean SAT variations and the external forcings suggests that the decadal–centennial global SAT changes in the past millennium were significantly driven by the effective radiative forcing agents. The results from the control run showed no significant decadal–centennial variations except for the peaks around 30 yr (not shown). On the other hand, the behavior of the internal mode differed from the forced variations. This may further demonstrate that the decadal–centennial variations in the forced simulation were primarily driven by the effective radiative forcing.

The seasonal and latitudinal dependence of volcanic aerosols was not taken into account in the simulation, which is potentially important for a realistic simulation of the last millennial climate. Analysis of proxy data indicates that tropical and high-latitude volcanic eruptions differ distinctly in their climate effects on regional climate (Shen et al., 2008). Therefore, further simulations driven by monthly and latitudinaldependent volcanic forcing data are needed for a better understanding of the effects of volcanic aerosols on global and regional climate.

Land-use change was also not included in our simulation. Although the global temperature changes due to land-use change may be small, regional effects may be discernable and thus should be included in future simulations. In addition, we did not conduct ensemble simulations in our study. It is essential to perform ensemble integrations in order to assess the internal variability in our future work.

The uncertainties in the reconstructions should also be ac-

knowledged. For example, our model response exhibited El Niño-like conditions during the MCA, while the reconstruction of Mann et al. (2005) indicated La Niña-like conditions. However, a recent reconstruction based on precipitation proxies indicates that the MCA may have seen El Niño-like conditions in the tropical Pacific (Yan et al., 2011). Thus how to provide solid reconstruction evidence for model comparisons also deserves further study.

Acknowledgements. This work was jointly supported by the National Natural Science Foundation of China (Grant No. 41305069), the Open Project Program of the Key Laboratory of Meteorological Disaster of Ministry of Education, Nanjing University of Information Science and Technology, and the National Program on Key Basic Research Project of China (Grant No. 2010CB951904)

REFERENCES

Ammann, C M., F. Joos, D. Schimel, B. L. Otto-Bliesner, and R. A. Tomas, 2007: Solar influence on climate during the past millennium: Results from transient simulations with the NCAR Climate System Model. *Proceedings of the National Academy of Sciences of the United States of America*, **104**(10), 3713–3718.

Bauer, E., M. Claussen, V. Brovkin, and A. Huenerbein, 2003: Assessing climate forcings of the Earth system for the past millennium. *Geophys. Res. Lett.*, **30**(6), 1276, doi: 101029/2002GL016639.

Bertrand, C., M-F. Loutre, M. Crucifix, and A. Berger, 2002: Climate of the last millennium: A sensitivity study. *Tellus*, **54**, 221–244.

Bonan, G. B., K. W. Oleson, M. Vertenstein, and S. Levis, 2002: The land surface climatology of the Community Land Model coupled to the NCAR Community Climate Model. *J. Climate*, **15**, 3123–3149.

Briegleb, B. P., C. M. Bitz, E. C. Hunke, and W. H. Lipscomb, 2004: Scientific description of the sea ice component in the Community Climate System Model: Version Three. NCAR Tech. Note NCARTN-463+STR, 70 pp.

Chang, C. P., Y. S. Zhang, and T. Li, 2000: Inter-annual and interdecadal variation of the East Asian summer monsoon and tropical Pacific SSTs. *J. Climate*, **13**, 4310–4340.

Christiansen, B., T. Schmith and P. Thejll, 2009: A surrogate ensemble study of climate reconstruction methods: stochasticity and robustness. *J. Climate*, **22**, 951–976.

Cobb, K M., C. D. Charles, H. Cheng, and R. L. Edwards, 2003: El Niño/Southern Oscillation and tropical Pacific climate during the last millennium. *Nature*, **424**, 271–276.

Cook, E R., J. Esper, and R. D'Arrigo, 2004: Extra-tropical Northern Hemisphere land temperature variability over the past 1000 years. *Quaternary Science Reviews*, **23**, 2063–2074.

Crowley, T., 2000: Causes of climate change over the past 1000 years. *Science*, **289**, 270–277.

Crowley, T J., S. K. Baum, K-Y. Kim, G. C. Hegerl, and W. T. Hyde, 2003: Modeling ocean heat content changes during the last millennium. *Geophys. Res. Lett.*, **30**(18), 1932, doi: 101029/2003GL017801.

D'Arrigo, R., R. Wilson, and G. Jacoby, 2006: On the long-term context for late twentieth century warming. *J. Geophys. Res.*, **111**(D3), doi: 101029/2005JD006352.

Dawdy, D., and N. Matalas, 1964: Statistical and probability analysis of hydrologic data, part III: Analysis of variance, covariance and time series. *Handbook of Applied Hydrology: A Compendium of Water-Resources Technology*, V. Chow Ed., McGraw-Hill, 868–890.

Esper, J., E. R. Cook, and F. H. Schweingruber, 2002: Low-frequency signals in long tree-ring chronologies for reconstructing past temperature variability. *Science*, **295**(5563), 2250–2253.

Fernandez-Donado, F., and Coauthors, 2013: Large-scale temperature response to external forcing in simulations and reconstructions of the last millennium. *Climate of the Past*, **9**, 393–421.

Ge, Q S., J. Y. Zheng, X. Q. Fang, Z. M. Man, X. Q. Zhang, P. Y. Zhang, and W. C. Wang, 2003: Winter half-year temperature reconstruction for the middle and lower reaches of the Yellow River and Yangtze River, China, during the past 2000 years. *The Holocene*, **13**(6), 933–940.

Ge, Q S., J. Y. Zheng Z. X. Hao, X. M. Shao, W. C. Wang, and J. Luterbacher 2010: Temperature variation through 2000 years in China: An uncertainty analysis of reconstruction and regional difference. *Geophys. Res. Lett.*, **37**, L03703, doi: 10.1029/2009GL04128.

Gerber, S., F. Joos, P. Brügger, T. Stocker, M. Mann, S. Sitch, and M. Scholze, 2003: Constraining temperature variations over the last millenium by comparing simulated and observed atmospheric CO_2. *Climate Dyn.*, **20**, 281–299.

Giorgi, F., and R. Francisco, 2000: Uncertainties in regional climate change prediction: A regional analysis of ensemble simulations with the $HADCM_2$ coupled AOGCM. *Climate Dyn.*, **16**, 169–182.

González-Rouco, F., H. Von Storch, and E. Zorita, 2003: Deep soil temperature as proxy for surface air-temperature in a coupled model simulation of the last thousand years. *Geophys. Res. Lett.*, **30**, 2116. doi: 101029/2003GL018264.

Goosse, H., H. Renssen, A. Timmermann, and R. S. Bradley, 2005: Internal and forced climate variability during the last millennium: a model-data comparison using ensemble simulations. *Quaternary Science Reviews*, **24**, 1345–1360.

Graham, N. E., and Coauthors, 2007: Tropical Pacific-mid-latitude teleconnections in medieval times. *Climatic Change*, **83**, 241–285.

Guo, Z., and T. J. Zhou, 2013: Why does FGOALS-gl reproduce a weak Medieval Warm Period but a reasonable Little Ice Age and 20th century warming? *Adv. Atmos. Sci.*, **30**, 1758–1770, doi: 10.1007/s00376-013-2227-8.

Hegerl, G. C., T J. Crowley, M Allen, W T. Hyde, H N. Pollack, J Smerdon, and E Zorita, 2007: Detection of human influence on a new, validated 1500-year temperature reconstruction. *J. Climate*, **20**, 650–666.

Hughes, M. K., and H. F. Diaz, 1994: Was there a "Medieval Warm Period", and if so, where and when? *Climatic Change*, **26**(2-3), 109–142.

Jansen, E., and Coauthors, 2007: *Climate Change 2007: The Physical Science Basis. Contribution of Working Group I to the Fourth Assessment Report of the Intergovernmental Panel on Climate Change*, Cambridge University Press, 748–845

Jones, P., and R. S. Bradley, 1992: Climatic variations over the last 500 years. *Climate since A. D.* 1500. R. Bradley, and P. Jones Eds., Routledge, 649–665.

Jones, P., and M. Mann, 2004: Climate over past millennia. *Rev.*

Geophys., **42**(2), RG2002, doi: 101029/2003RG000143.

Jungclaus, J. H., and Coauthors, 2010: Climate and carbon-cycle variability over the last millennium. *Climate of the Past*, **6**, 723–737.

Kaufman, D. S., and Coauthors, 2009: Recent warming reverses long-term Arctic cooling. *Science*, **325**, 1236–1339.

Lean, J., J. Beer, and R. Bradley, 1995: Reconstruction of solar irradiance since 1610: Implications for climate change. *Geophys. Res. Lett*., **22**(23), 3195–3198, doi: 10.1029/95GL 03093.

Ljungqvist, F. C., 2010: A new reconstruction of temperature variability in the extra-tropical Northern Hemisphere during the last two millennia. *Geografiska Annaler: Series A*, *Physical Geography*, **92**, 339–351.

Liu, H L. X. H. Zhang, W. Li, Y. Q. Yu, and R. C. Yu, 2004: An eddy-permitting oceanic general circulation model and its preliminary evaluation. *Adv. Atmos. Sci*., **21**, 675–690.

Liu, J., B. Wang, Q. H. Ding, X. Y. Kuang, W. Soon, and E. Zorita, 2009: Centennial variations of the global monsoon precipitation in the last millennium: Results from ECHO-G model. *J. Climate*, **22**, 2356–2371.

Liu, J., B. Wang, H. L. Wang, X. Y. Kuang, and R. Y. Ti, 2011: Forced response of the East Asian summer rainfall over the past millennium: Results from a coupled model simulation. *Climate Dyn*., **36**, 323–336, doi: 10.1007/s00382-009-0693-6.

Man, W. M., and T. J. Zhou, 2011: Forced response of atmospheric oscillations during the last millennium simulated by a climate system model. *Chinese Science Bulletin*, **56**, 3042–3052.

Man, W M., T Zhou, J Zhang, and B. Wu, 2011: The 20th century climate simulated by LASG/IAP climate system model FGOALS_gl. *Acta Meteorologica Sinica*, **69**(4), 644–654. (in Chinese)

Man, W. M., T. J. Zhou and J. H. Jungclaus, 2012: Simulation of the East Asian summer monsoon during the Last Millennium with the MPI Earth System Model. *J. Climate*, **22**(25), 7852–7866.

Mann, M. E., R. S. Bradley, and M. K. Hughes, 1999: Northern hemisphere temperatures during the past millennium: Inferences, uncertainties, and limitations. *Geophys. Res. Lett*., **26**, 759–762.

Mann, M. E., M. A. Cane, S. E. Zebiak, and A. Clement, 2005: Volcanic and solar forcing of the tropical Pacific over the past 1000 years. *J. Climate*, **18** 447–456.

Mann, M. E., and Coauthors, 2009: Global signatures and dynamical origins of the little ice age and Medieval Climate Anomaly. *Science*, **326**, 1256–1260.

Moberg, A., D. M. Sonechkin, K. Holmgren, N. M. Datsenko and W. Karlén, 2005: Highly variable Northern Hemisphere temperatures reconstructed from low- and high-resolution proxy data. *Nature*, **433**(7026), 613–617.

Osborn, T. J., S. C. B. Raper, and K. R. Briffa, 2006: Simulated climate change during the last 1, 000 years: Comparing the ECHO-G general circulation model with the MAGICC simple climate model. *Climate Dyn.*, **27**, 185–197.

Overpeck, J., and Coauthors, 1997: Arctic environmental change of the last four centuries. *Science*, **278**(5341), 1251–1256.

Peng, Y. B., Y. Xu, and L. Y. Jin, 2009: Climate changes over eastern China during the last millennium in simulations and reconstructions. *Quaternary International*, **208**, 11–18.

Rutherford, S., M. E. Mann, T. J. Osborn, R. S. Bradley, K. R. Briffa M. K. Hughes, and P. D. Jones, 2005: Proxy-based Northern Hemisphere surface temperature reconstructions: Sensitivity to method, predictor network, target season, and target domain. *J. Climate*, **18**(13), 2308–2329.

Servonnat, J., P. Yiou, M. Khodri, D. Swingedouw, and S. Denvil, 2010: Influence of solar variability, CO_2 and orbital forcing between 1000 and 1850 AD in the IPSLCM4 model. *Climate of the Past*, **6**, 445–460.

Shen, C M., W. C. Wang, Z. X. Hao, and W. Gong, 2008: Characteristics of anomalous precipitation events over eastern China during the past five centuries. *Climate Dyn*., **31**, 463–476.

Shen, S., and K. M. Lau, 1995: Biennial oscillation associated with the East Asian summer monsoon and tropical Pacific sea surface temperature anomalies. *J. Meteor. Soc. Japan*, **73**, 105–124.

Schmidt, G., and Coauthors, 2011: Climate forcing reconstructions for use in PMIP simulations of the last millennium (v1. 0). *Geoscientific Model Development* **4**, 33–45.

Smerdon, J E., A. Kaplan, D. N. Chang, and M. N. Evans, 2010: A pseudoproxy evaluation of the CCA and RegEM methods for reconstructing climate fields of the last millennium. *J. Climate*, **23**, 4856–4880.

Tan, M., T. S. Liu, J. Z. Hou, X. G. Qin, H. C. Zhang, and T. Y. Li, 2003: Cyclic rapid warming on centennial-scale revealed by a 2650-year stalagmite record of warm season temperature. *Geophys. Res. Lett*., **3**(12), 1617, doi: 101029/2003GL017352.

Trouet, V., J. Esper, N. E. Graham, A. Baker, J. D. Scourse, and D. C Frank, 2009: Persistent positive North Atlantic Oscillation mode dominated the Medieval Climate Anomaly. *Science*, **324**(5923), 78–80.

Wang, S W., X. Y. Wen, Y. Luo, W. J. Dong, Z. C. Zhao, and B. Yang, 2007: Reconstruction of temperature series of China for the last 1000 years. *Chinese Science Bulletin*, **52**, 3272–3280. (in Chinese)

Wen, X Y. T. J. Zhou, S. W. Wang, B. Wang, H. Wan, and J. Li, 2007: Performance of a reconfigured atmospheric general circulation model at low resolution. *Adv. Atmos. Sci*., **24**, 712–728, doi: 10.1007/s00376-007-0712-7.

Yan, H., L. G. Sun, Y. H. Wang, W. Huang, S. C. Qiu, and C. Y. Yang, 2011: A record of the Southern Oscillation Index for the past 2, 000 years from precipitation proxies. *Nature Geoscience*, **4**, 611–614, doi: 101038/NGEO1231.

Yang, B., A. Braeuning, K. R. Johnson, and Y. F. Shi, 2002: General characteristics of temperature variation in China during the last two millennia. *Geophys. Res. Lett*., **29**(9), 1324, doi: 101029/2001GL014485.

Yoshimori, M., T. F. Stocher, C. C. Raible and M. Renold, 2005: Externally forced and internal variability in ensemble climate simulations of the Maunder Minimum. *J. Climate*, **18**, 4253–4268.

Zebiak, S. E., and M. A. Cane, 1987: A model El Niño/Southern Oscillation. *Mon. Wea. Rev*., **115** 2262–2278.

Zhang, J., L. Li, T. J. Zhou, and X. G. Xin, 2013: Variation of surface temperature during the last millennium in a simulation with the FGOALS_gl climate system model. *Adv. Atmos. Sci.*, **30**, 699–712, doi: 10.1007/s00376-013-2178-0.

Zhang, P Z., and Coauthors, 2008: A test of climate, sun, and culture relationships from an 1810-Year Chinese cave record. *Science*, **322**, 940–942.

Zhou, T. J., and R. C. Yu, 2006: Twentiethcentury surface air temperature over China and the globe simulated by coupled climate models. *J. Climate*, **19**(22), 5843–5858.

Zhou, T. J., B. Wu, X. Y. Wen, L. J. Li, and B. Wang, 2008: A fast version of LASG/IAP climate system model and its 1000-year control integration. *Adv. Atmos. Sci*., **25**(4), 655–672, doi: 10.1007/s00376-008-0655-7.

Zhou, T. J., B. Li, W. M. Man, L. X. Zhang, and J. Zhang, 2011: A comparison of the medieval warm period, little ice age and 20th Century warming simulated by the FGOALS climate system model. *Chinese Science Bulletin*, **56**, 3028–3041.

Zhou, T J., F. F. Song, and X. L. Chen, 2013: Historical evolutions of global and regional surface air temperature simulated by FGOALS-s2 and FGOALS-g2: How reliable are the model results? *Adv. Atmos. Sci.*, **30**, 638–657, doi: 10.1007/s00376-013-2205-1.

Zorita, E., J. F. González-Rouco, H. von Storch, J. P. Montávez, and F. Valero, 2005: Natural and anthropogenic modes of surface temperature variations in the last thousand years. *Geophys. Res. Lett*., **32**, L08707, doi: 101029/2004GL021563.